

## Enhancement of drag and mixing in a dilute solution of rodlike polymers at low Reynolds numbers

L. Puggioni , G. Boffetta, and S. Musacchio \*

*Dipartimento di Fisica and INFN, Università degli Studi di Torino, via P. Giuria 1, 10125 Torino, Italy*



(Received 29 December 2021; accepted 22 July 2022; published 17 August 2022)

We study the dynamics of a dilute solution of rigid rodlike polymers in a viscous fluid at low Reynolds numbers by means of numerical simulations of a simple rheological model. We show that the rotational dynamics of polymers destabilizes the laminar flow and causes the emergence of a turbulent-like chaotic flow with a wide range of active scales. This regime displays an increased flow resistance, corresponding to a reduced mean flow at fixed external forcing, as well as an increased mixing efficiency. The latter effect is quantified by measuring the decay of the variance of a scalar field transported by the flow. By comparing the results of numerical simulations of the model in two and three dimensions, we show that the phenomena observed are qualitatively independent on the dimensionality of the system, but the effects of polymer are, in general, stronger in two dimensions. This dimensional effect is explained in terms of the different rotational degrees of freedom of the rods.

DOI: [10.1103/PhysRevFluids.7.083301](https://doi.org/10.1103/PhysRevFluids.7.083301)

### I. INTRODUCTION

The addition of small amounts of polymers in a fluid causes dramatic effects on the mechanical properties of the solution. At high Reynolds numbers, it is well known that polymers reduce the turbulent drag compared to that of the solvent alone [1]. The discovery of the phenomenon of drag reduction motivated the efforts of the scientific community to investigate the dynamics of dilute polymer solutions (see, e.g., the reviews in Refs. [2–4]). More recently, it has been discovered that polymer additives alter significantly also flows at low Reynolds numbers. In this case, even though the Reynolds stress is negligible, the elastic stress gives rise to instabilities when the elasticity of polymers is large enough. The growth of these instabilities eventually generates a spatiotemporal chaotic regime which is called “elastic turbulence” [5]. In this regime, the mixing efficiency of the flow is strongly enhanced, because the velocity field develops chaotic structures at small scales, and the flow displays a power-law energy spectrum [6–8]. This phenomenon is extremely useful to increase the mixing in microfluidic applications, in which the Reynolds numbers are typically very low and the diffusive mixing is weak.

Although most of the studies of these phenomena have been performed with elastic polymers, the described effects can originate also from rigid rodlike polymers. One advantage of using rodlike polymers in applications is that the degradation due to large strains is weaker for rodlike polymers than for elastic polymers [9]. At large Reynolds numbers, it has been shown that the drag reduction obtained by elastic- and rigid-polymers is remarkably similar [10–14]. At small Reynolds numbers, recent numerical studies performed in two dimensions demonstrated that the addition of rigid polymers originates a chaotic regime similar to elastic turbulence [15] characterized by enhanced mixing [16].

---

\*Corresponding author: [stefano.musacchio@unito.it](mailto:stefano.musacchio@unito.it)

In general, the chaotic dynamics at low Reynolds number is expected to be qualitatively similar in two-dimensional (2D) and three-dimensional (3D) flows. This is at odds with the high-Reynolds regime, in which the dimensionality of the flow has dramatic consequences, namely the reversal of the turbulent cascade of kinetic energy [17,18]. The possibility to use 2D studies for the modeling of 3D applications offers considerable advantages, such as the reduction of computational costs and the simplification of the experimental setup. Nonetheless, changing the dimensionality of the system can produce quantitative discrepancies between 2D and 3D results. As an example, recent numerical studies of Rayleigh-Taylor convection in porous media observed density plumes more elongated and thinner in 2D than in 3D. This difference causes a faster growth of the mixing layer in 2D [19,20]. The comparison of 3D and 2D studies is therefore crucial to reveal quantitative effects of the dimensionality on low Reynolds number flows.

For this purpose, here we extend the investigation of the chaotic regime in viscous solutions of rodlike polymers to 3D flows. We present the results of 3D numerical simulations of the rheological model considered in Ref. [15] and we compare them with 2D simulations performed with identical parameters. At a qualitative level, we find that the phenomenology of 2D and 3D systems is similar. Augmenting the concentration of polymers we find an increase of the flow resistance, quantified by the friction factor, as well as an enhanced mixing efficiency. The latter is measured by the decay rate of the variance of a scalar field transported in the flow. Nonetheless, an accurate comparison reveals remarkable quantitative differences between 3D and 2D simulations. In particular, we show that the effects of polymers in 2D is stronger than in 3D. We provide an interpretation of this dimensional effect in terms of the rotational degrees of freedom of polymers. We also discuss the possibility of a mapping between the 2D and 3D results, which is obtained by rescaling the concentration of polymers.

The paper is organized as follows. In Sec. II we present the Eulerian model for the dilute rods suspension. The details of the numerical simulations are reported in Sec. III. In Sec. IV we discuss the results of 3D simulations and the comparison with 2D simulations. Section V is devoted to the conclusions.

## II. EULERIAN MODEL FOR A DILUTE RODS SUSPENSION

We consider an Eulerian model for a dilute suspension of inertialess rodlike polymers transported by an incompressible velocity field  $\mathbf{u}(\mathbf{x}, t)$ . The polymer phase is described by a unit-trace symmetric tensor  $R_{i,j}(\mathbf{x}, t) = \langle n_i n_j \rangle_{\mathcal{V}}$ , which is defined as the average of the orientation vectors  $\mathbf{n}$  of individual polymers over an infinitesimal volume element  $\mathcal{V}$  at position  $\mathbf{x}$  and time  $t$  [21]. The dynamics of the suspension is determined by the following coupled equations:

$$\partial_t u_i + u_k \partial_k u_i = -\partial_i p + \nu \partial^2 u_i + \partial_k \sigma_{ik} + f_i, \quad (1a)$$

$$\partial_t R_{ij} + u_k \partial_k R_{ij} = (\partial_k u_i) R_{kj} + R_{ik} (\partial_k u_j) - 2R_{ij} (\partial_l u_k) R_{kl}, \quad (1b)$$

where  $p(\mathbf{x}, t)$  is the pressure,  $\nu$  is the kinematic viscosity of the solvent fluid, and  $\mathbf{f}(\mathbf{x}, t)$  is the body-force which sustains the flow. The form of the polymer stress tensor  $\sigma_{ij}$  is based on a quadratic approximation proposed by Doi and Edwards [21]  $\sigma_{ij} = 6\nu\eta R_{ij} (\partial_l u_k) R_{kl}$ . The intensity of the polymer feedback on the flow is determined by the dimensionless parameter  $\eta$  which is proportional to the polymer concentration. We remark that Eq. (1b) can also contain a term produced by the orientational diffusion of polymers [21]. The effects of Brownian rotations of the rods can be safely disregarded when the characteristic Brownian rotational time  $t_B$  is much larger than the dynamical rotational time  $t_L$  determined by the velocity gradients [22] (i.e., when the rotational Péclet number  $Pe = t_B/t_L$  is large). For an elongated particle of length  $\ell$  and aspect ratio  $r$  in a solvent with density  $\rho$  at temperature  $T$ , the Brownian time is given by  $t_B = (\pi \rho \nu \ell^3) / \{3k_B T [\ln(r) - 0.8]\}$  where  $k_B$  is the Boltzmann constant [21,23]. The dynamical time can be estimated as  $t_L \approx (L^2/\nu)\text{Re}^{-1}$ , where  $L$  is the characteristic scale of the flow and  $\text{Re}$  is the Reynolds number. As an example, for an experiment in a microchannel of width  $L \approx 1$  mm at  $\text{Re} \approx 1$ , with rigid fibers of length  $\ell = 5 \mu\text{m}$

and aspect ratio  $r = 10$  in water at  $T = 300$  K, the dynamical time  $t_L \approx 1$  s is much smaller than the Brownian time  $t_B \approx 20$  s. Having these applications in mind, in the following we omit the Brownian term. We also remind that numerical simulations at large Reynolds numbers have shown that model (1) is able to reproduce the main features of turbulent drag reduction in channel flows [12,14,24,25].

We focus here on a 3D viscous shear flow sustained by the Kolmogorov body force  $\mathbf{f}(\mathbf{x}) = [F \cos(Kz), 0, 0]$ , where  $F$  is the amplitude and  $K$  is the wave number of the force. In the absence of polymers ( $\eta = 0$ ) this force produces the stationary laminar solution  $\mathbf{u}(\mathbf{x}) = [U_0 \cos(Kz), 0, 0]$  with  $U_0 = F/(K^2\nu)$ , which is linearly stable if the Reynolds number  $\text{Re} = U_0/(\nu K)$  is smaller than the critical value  $\text{Re}_c = \sqrt{2}$  [26]. This flow has been first proposed by Kolmogorov as a model to understand the transition to turbulence. It displays the interesting feature that the mean velocity profile remains monochromatic even in the turbulent regime, i.e.,  $\bar{\mathbf{u}}(z) = [U \cos(Kz), 0, 0]$  [27]. Here and in the following the overbar  $\bar{[\cdot]}$  denotes the average over time  $t$  and over the  $x$  and  $y$  coordinates. In analogy with the case of channel flows, the presence of a nonvanishing mean velocity profile allows us to define the turbulent drag coefficient  $f = F/(KU^2)$  in terms of the amplitude  $U$  of the mean flow, which in the turbulent regime is smaller than the laminar solution  $U_0$ . This property has been exploited to study the dependence on  $\text{Re}$  of the turbulent drag in bulk flows [27], and to investigate how the drag is affected by the presence of elastic polymers [28] or inertial particles [29].

In the presence of rodlike polymers ( $\eta > 0$ ), the stationary solution of Eq. (1) requires, for the conformation tensor,  $R_{i3} = R_{3i} = 0$  and  $\partial_x R_{ij} = 0$ , that is, polymers are oriented in the  $x$ - $y$  plane and their orientation can depend on the  $y$  and  $z$  coordinates only. For the velocity field, the stationary solution is the laminar Kolmogorov flow  $[U_0 \cos(Kz), 0, 0]$  with amplitude  $U_0 = F/(K^2\nu)$  independent on the polymer concentration. This is remarkably different from the case of the viscoelastic model, in which polymers affect the amplitude of the laminar flow [28].

### III. NUMERICAL SIMULATIONS

We performed a set of numerical simulations of Eq. (1) on a triply cubic periodic domain of size  $L = 2\pi$ . Simulations are performed by using a pseudospectral code which discretizes the velocity and conformation tensor fields on a regular grid of  $N^3 = 256^3$  gridpoints. Since Eq. (1) contains terms which are cubic in the fields, the code performs a 1/2 dealiasing at each time step [30]. Time integration uses a fourth-order Runge-Kutta scheme with implicit integration of the linear dissipative terms and the time step is fixed by the resolution of the rotational dynamics of the conformation tensor. In all the simulations the viscosity is set to  $\nu = 1$  and the flow is sustained by the Kolmogorov force  $\mathbf{f}(\mathbf{x}) = [F \cos(Kz), 0, 0]$ , with forcing wave number  $K = 4$  and forcing amplitude  $F = \nu^2 K^3$ , such that, in absence of polymers ( $\eta = 0$ ), the laminar flow is stable with Reynolds number  $\text{Re} = U_0/(\nu K) = 1$ . The feedback coefficient is varied from  $\eta = 5$  to  $\eta = 8$ . Experimentally this corresponds, for the case of an aqueous solution of xanthan gum, to concentrations in the range of 73–102 wppm [25]. The values of  $\eta$  considered are small enough to be in the dilute regime but also large enough to ensure that the system is far from the transition from the laminar to the chaotic flow observed in [15]. A diffusive term  $\kappa \partial^2 R_{ij}$  with  $\kappa = 4 \times 10^{-3}$  is added to Eq. (1b) to improve the numerical stability [31]. All the results are made dimensionless by using the forcing wave number  $K$ , the laminar velocity amplitude  $U_0$  and the laminar time  $T_0 = 1/(KU_0)$ . For a quantitative comparison between the 2D and the 3D versions of the model, we also performed additional numerical simulations of Eq. (1) in two dimensions with the same parameters of the 3D runs.

At time  $t = 0$  we initialize the velocity field to the fixed-point laminar solution while the components of the tensor  $R$  are distributed randomly with isotropic distribution. The time evolution of the kinetic energy  $E = \frac{1}{2} \langle |\mathbf{u}|^2 \rangle$  is shown in Fig. 1 for two simulations with  $\eta = 6$  and  $\eta = 8$  (here and in the following  $\langle \cdot \rangle$  denotes the average over the whole volume). The injection of polymers strongly affects the velocity field and the energy is almost reduced to zero. Energy further increases back to the laminar value (at  $t \simeq 200T_0$  in Fig. 1) where polymeric instabilities develop and eventually

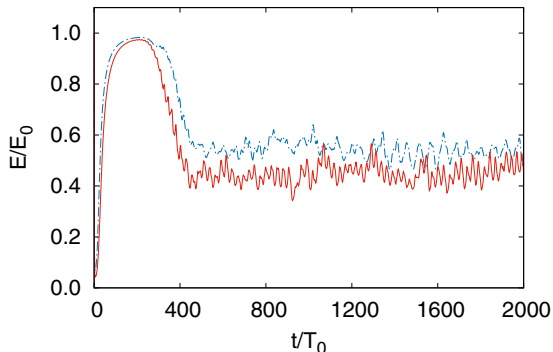


FIG. 1. Kinetic energy  $E$ , normalized with the laminar energy  $E_0$ , for two simulations in 3D with  $\eta = 6$  (blue dashed line) and  $\eta = 8$  (red solid line). In both cases the initial condition is the laminar fixed point with  $E(0) = E_0$ .

the system reaches a statistically stationary chaotic state (at  $t \geq 500T_0$ ) with an energy which is considerably smaller than the one of the laminar flow  $E_0 = \frac{1}{2}U_0^2$ . In this regime, the kinetic energy displays rapid oscillations whose frequency increases with the polymer concentration, while the average value of  $E$  decreases at increasing  $\eta$ .

For each set of the parameters, we performed three independent simulations with different realizations of the initial random configuration of the conformation tensor. While the duration of the initial transient depends on the realization, in the subsequent chaotic regime different realizations are statistically equivalent and they are averaged to increase the statistical accuracy of the results. All the results presented are obtained in this statistically stationary regime.

Figure 2 shows three sections of the velocity components  $u_x$ ,  $u_y$ , and  $u_z$  in the plane  $x$ - $z$  at fixed  $y$  from the simulation with  $\eta = 7$  in the chaotic regime. The structure of the Kolmogorov flow remains visible in the  $u_x$  field, with superimposed irregular fluctuations at small scales. The velocity fluctuations are clearly evident in the  $u_y$  and  $u_z$  fields, where the mean flow is absent. We remark that the fluctuations in the  $u_x$  field qualitatively resemble the elastic waves observed in viscoelastic flows [32,33].

## IV. RESULTS

### A. Statistics of the velocity

One relevant property of the Kolmogorov flow is that it maintains a monochromatic mean flow  $\langle u_x \rangle = U \cos(Kz)$  also in the chaotic and in the turbulent regimes. This feature is confirmed even

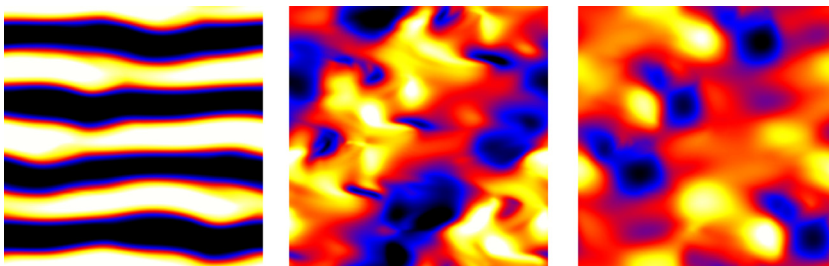


FIG. 2. Vertical sections in the  $x$ - $z$  plane of the velocity components  $u_x$ ,  $u_y$ ,  $u_z$  (from left to right) in the 3D chaotic regime for  $\eta = 7$ . The color scale ranges from  $-3u'_i$  (black) to  $3u'_i$  (white), where  $u'_i$  are the root-mean-square (rms) values of the velocity fluctuations.

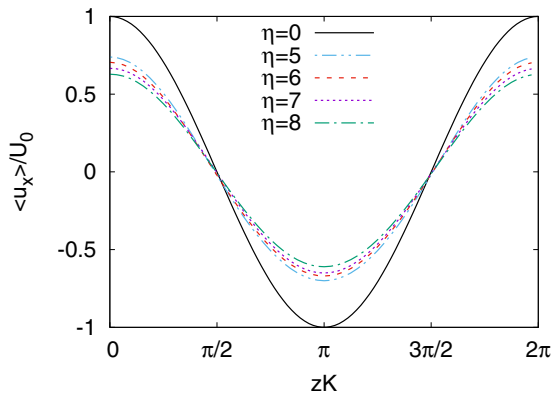


FIG. 3. Profiles of the mean velocity  $\langle u_x(z) \rangle$  averaged over  $x$ ,  $y$  and time, in 3D simulations with different values of  $\eta$ . The solid black line corresponds to the laminar solution of the Newtonian fluid at  $\eta = 0$ .

in the presence of polymers, as shown in Fig. 3 where we plot the average velocity profile from the simulations at different concentrations. We observe that the amplitude of the mean flow is reduced with respect to the laminar solution, consistently with what shown in Fig. 1, as a consequence of the chaotic motion induced by polymers.

It is therefore natural to decompose the velocity field in a mean (monochromatic) component and fluctuations as

$$\mathbf{u}(\mathbf{x}) = U[\cos(Kz), 0, 0] + \mathbf{u}'(\mathbf{x}). \quad (2)$$

Table I reports the values of the root-mean-square (rms) velocity fluctuations together with the amplitude of the mean flow and other relevant quantities.

Figure 4(a) confirms that the amplitude of the mean flow is significantly reduced with respect to the laminar case and that this effect is stronger at increasing values of the concentration parameter  $\eta$ . The rms values of velocity fluctuations are, on the contrary, weakly dependent on  $\eta$ . We notice that fluctuations along streamwise direction  $u'_x$  are larger than those in the  $y$  and  $z$  directions and the fluctuations in the spanwise direction  $u'_y$  are much smaller. This suggests that, even in the chaotic regime, the flow remains approximately two-dimensional.

### B. Drag and momentum budget

To better understand the effect of polymers on the mean flow we consider the momentum budget. By averaging the first component of Eq. (1) over  $x$ ,  $y$  in stationary conditions we obtain the stress

TABLE I. Parameters of the 3D simulations.  $U$  is the amplitude of the mean longitudinal velocity,  $S$  the amplitude of the mean Reynolds stress, and  $\Sigma$  that of the mean polymer stress.  $u'_x$ ,  $u'_y$ , and  $u'_z$  are the rms values of the three components of velocity fluctuations.  $\varepsilon_I$  is the mean energy input,  $\varepsilon_v$  the viscous energy dissipation, and  $\varepsilon_p$  the mean polymer dissipation.

$\eta$	$U$	$S$	$\Sigma$	$u'_x$	$u'_y$	$u'_z$	$\varepsilon_I$	$\varepsilon_v$	$\varepsilon_p$
5	2.87	0.10	4.40	0.64	0.12	0.40	91.9	74.8	17.1
6	2.74	0.10	5.02	0.63	0.13	0.39	87.2	68.6	18.6
7	2.63	0.10	5.57	0.64	0.16	0.39	83.2	63.6	19.6
8	2.48	0.09	6.08	0.69	0.18	0.40	78.8	58.3	20.6

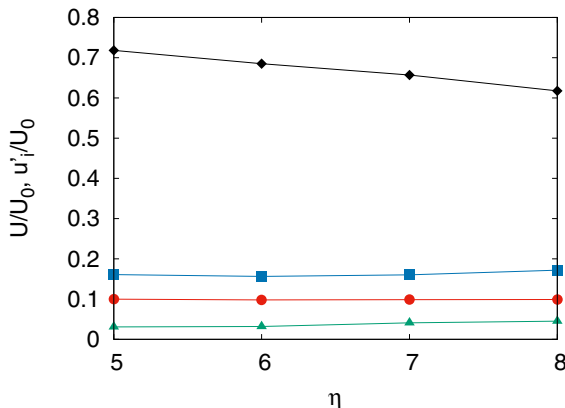


FIG. 4. Mean velocity profiles  $U$  (black diamonds) and components of rms velocity fluctuations ( $u'_x$  blue squares,  $u'_y$  green triangles,  $u'_z$  red circles) in 3D simulations with different values of  $\eta$ .

budget

$$\partial_z \Pi_r = \partial_z (\Pi_v + \Pi_p) + f_x, \quad (3)$$

where  $\Pi_r = \overline{u_x u_z}$  is the Reynolds stress,  $\Pi_v = \nu \partial_z \overline{u_x}$  the viscous stress, and  $\Pi_p = \overline{\sigma_{xz}}$  the polymer stress. In the statistically stationary state all these quantities have a monochromatic profile

$$\Pi_r = S \sin(Kz), \quad \Pi_v = -\nu K U \sin(Kz), \quad \Pi_p = -\Sigma \sin(Kz), \quad (4)$$

and therefore Eq. (3) becomes an algebraic equation for the coefficients

$$SK + \nu K^2 U + \Sigma K = F. \quad (5)$$

The dimensionless version of the momentum budget is obtained by dividing all the terms of Eq. (5) by  $KU^2$  and defining the friction coefficient  $f = F/(KU^2)$ , which quantifies the ratio between the work done by the force and the kinetic energy of the mean flow, the Reynolds stress coefficient  $s = S/U^2$  and the polymer stress coefficient  $\sigma = \Sigma/U^2$ :

$$f = \frac{1}{\text{Re}} + s + \sigma. \quad (6)$$

In laminar conditions we have  $s = \sigma = 0$  and  $f = 1/\text{Re}$ . Figure 5 shows that increasing the concentration of polymers produces a growth of the friction factor with respect to the laminar case which is mostly due to the increment of the polymer stress and partly to a weaker growth of the viscous stress. The Reynolds stress remains in all cases negligible, showing that inertial terms do not contribute to the transfer of momentum.

By definition, the drag coefficient  $f$  is linked to the Reynolds number by  $f = \text{Re}_0/\text{Re}^2$  where  $\text{Re}_0 = U_0/K\nu = F/K^3\nu^2$ . Polymers have therefore two complementary effects: they reduce the Reynolds number of the flow and increase its resistance. Note that the contribution of the viscous stress to the increase of the drag coefficient is subdominant ( $\propto 1/\text{Re}$ ) with respect to that of the polymer stress ( $\propto 1/\text{Re}^2$ ). This is clearly shown in Fig. 6 in which the friction factor  $f$  is plotted as a function of  $\text{Re}$  for the different values of  $\eta$ . Since both  $f$  and  $\text{Re}$  do not depend explicitly on  $\eta$ , points corresponding to simulations at the same  $F$  and  $\nu$  lie on the line  $\text{Re}_0/\text{Re}^2$ . The point at  $\text{Re} = 1$  corresponds to the laminar fixed point, which is stable in the absence of polymers. We remark that this plot is done at fixed forcing  $F$ . The different Reynolds numbers are a consequence of the different mean velocities produced at various  $\eta$ .

The inset of Fig. 6 shows how the effective viscosity  $\nu_{\text{eff}} \equiv F/(K^2U)$  increases with the mean shear rate  $\dot{\gamma} = KU$ , by changing the amplitude  $F$  of the forcing at fixed polymer concentration

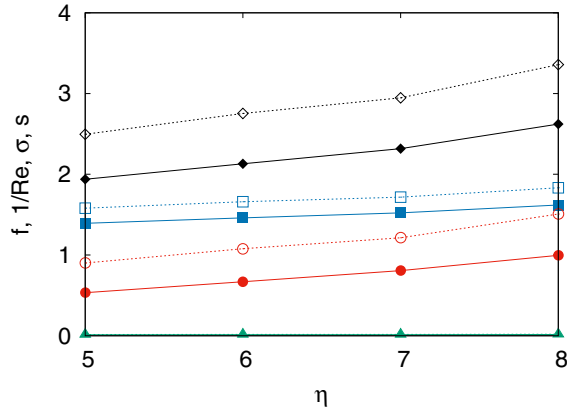


FIG. 5. Friction factor  $f$  (black diamonds) normalized viscous stress  $1/Re$  (blue squares), polymer stress coefficient  $\sigma$  (red circles) and Reynolds stress coefficient  $s$  (green triangles), as function of  $\eta$ . Filled symbols are for the three-dimensional DNS, empty ones are for the two-dimensional DNS.

(data from two-dimensional simulations). In this range of values, the polymer solution displays shear-thickening behavior.

### C. Energy budget

Additional information regarding the effects of polymers on the flow is obtained by the analysis of the energy budget. By multiplying Eq. (1) by  $\mathbf{u}$  and integrating over the volume we get the balance equation for the mean kinetic energy (we note that, unlike the case of elastic polymers, we cannot

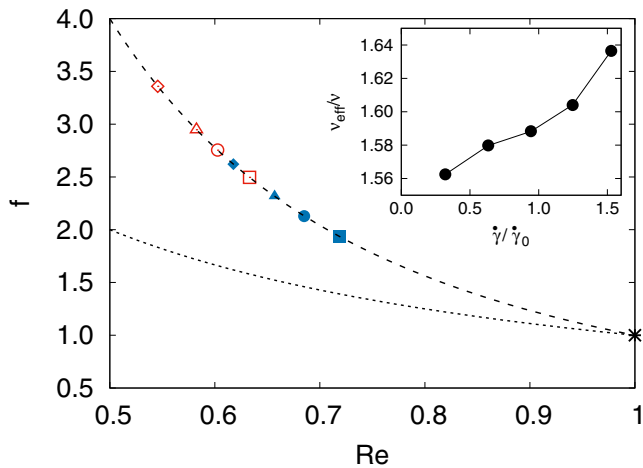


FIG. 6. Friction factor  $f$  as a function of  $Re$  in the 3D (blue, filled symbols) and 2D (red, empty symbols) simulations at concentrations  $\eta = 5$  (squares),  $\eta = 6$  (circles),  $\eta = 7$  (triangles),  $\eta = 8$  (diamonds). The black asterisk at  $Re = 1$  represents the laminar fixed point at  $\eta = 0$ . The dashed line represents the curve  $f = Re_0/Re^2$  while the dotted line is the laminar law  $f = 1/Re$ . Inset: effective viscosity  $\nu_{\text{eff}}$  as a function of the mean shear rate  $\dot{\gamma}$  for 2D simulations with  $\eta = 5$ .

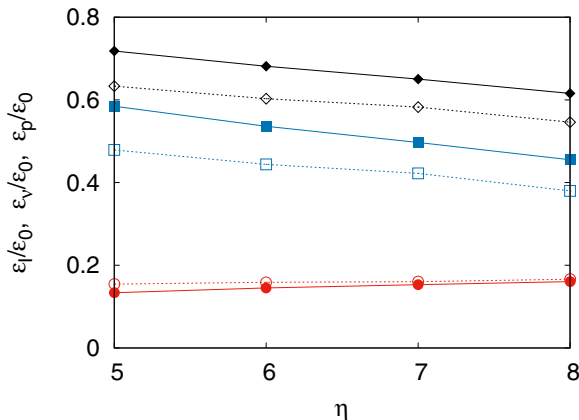


FIG. 7. Mean values of energy input  $\varepsilon_I$  (black diamonds), viscous dissipation  $\varepsilon_v$  (blue squares), and polymer dissipation  $\varepsilon_p$  (red circles), as function of  $\eta$ . Filled symbols are for the three-dimensional DNS, empty ones are for the two-dimensional DNS.

associate a deformation energy to rigid polymers)

$$\frac{d}{dt}\langle E \rangle = \varepsilon_I - \varepsilon_v - \varepsilon_p, \quad (7)$$

where  $\varepsilon_I = \langle \mathbf{f} \cdot \mathbf{u} \rangle = FU/2$  is the mean energy input,  $\varepsilon_v = \langle \nu |\nabla \mathbf{u}|^2 \rangle$  the mean viscous dissipation rate, and  $\varepsilon_p = \langle \sigma_{ij} \partial_j u_i \rangle$  is an additional dissipation of kinetic energy due to the coupling with polymers. We remark that the local values of the term  $\sigma_{ij} \partial_j u_i$  can be either positive or negative, meaning that polymers can locally either give or subtract energy from the flow. Nonetheless the volume average of  $\varepsilon_p$  is always negative, indicating that the global effect of polymers is dissipative. Physically, this is due to the fact that the coupling between rods and the fluid is due to viscous forces at the molecular scale, whose mean effect is to dissipate a fraction of the kinetic energy [21].

In the statistical steady state, averaging over sufficiently long times, the energy can be considered constant, and therefore we have the energy balance  $\varepsilon_I = \varepsilon_v + \varepsilon_p$ . These quantities are shown in Fig. 7, normalized with the mean energy input of the laminar flow  $\varepsilon_0 = FU_0/2$ . We observe a slight increase in the polymer dissipation as the concentration coefficient increases, but the main effect of polymers is a suppression of the energy input provided by the constant forcing as a consequence of the reduction of the mean flow amplitude. This is consistent with the results plotted in Fig. 1 showing that kinetic energy is reduced at increasing polymer concentration. Figure 7 indicates that for all values of  $\eta$ , energy is mostly dissipated by viscosity. Therefore, we expect that the small scale properties of the flow are weakly affected by the polymer concentration.

To investigate in details this point, in Fig. 8 we plot the kinetic energy spectra in stationary conditions and for the different values of concentration. Note the peak of the spectra at the forcing wave number  $K$  (the only active wave number in the laminar case). We observe very small variations of the spectrum with  $\eta$ , mostly concentrated at small wave numbers (since the total energy changes with  $\eta$ ). At large wave numbers the spectra display a power law behavior  $E(k) \sim k^{-\alpha}$  with  $\alpha \simeq 4.8$ , an indication of the presence of fluctuations at all scales. The fact that the power spectrum is steeper than  $k^{-3}$  implies that the velocity field is smooth in this regime, similarly to what observed in elastic turbulence [5].

#### D. Mixing properties

The presence of velocity fluctuations over a wide range of spatial scales has a strong influence on the mixing efficiency of the flow. To address this point we studied the mixing of a passive scalar

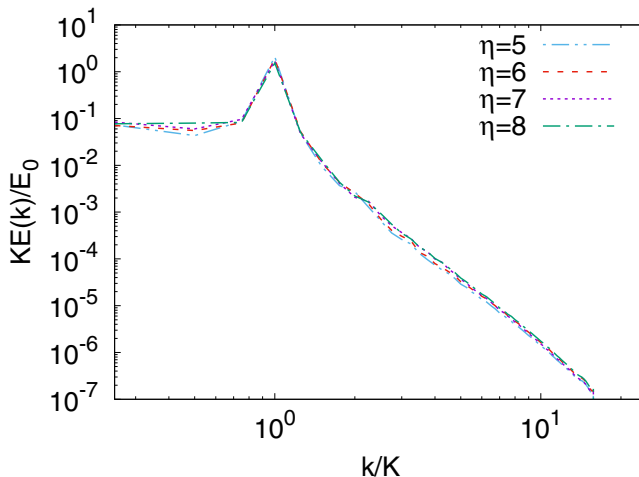


FIG. 8. Time averaged, kinetic energy spectra as a function of wave number from 3D simulations with different values of  $\eta$ .

by simultaneously integrating the equation for a scalar field  $\theta(\mathbf{x}, t)$  transported by the velocity field  $\mathbf{u}$  obtained from Eqs. (1)

$$\partial_t \theta + u_k \partial_k \theta = D \partial^2 \theta, \quad (8)$$

where  $D$  is the molecular diffusivity, which is set to  $D = 2 \times 10^{-3}$  in the simulations. The integration of Eq. (8) is obtained with the same pseudospectral method discussed in Sec. III. It starts at an arbitrary time in the stationary regime of chaotic flow. We chose a monochromatic initial condition for  $\theta$ , with the same periodicity of the mean flow  $\theta(\mathbf{x}, 0) = \theta_0 \cos(Kz)$ . In absence of polymers, with this initial condition the mixing is due exclusively to molecular diffusion because the gradients of the scalar field  $\nabla \theta$  are orthogonal to the laminar velocity field. In particular, for  $\eta = 0$  the scalar field remains monochromatic, while its variance (as well as the variance of its gradients) decays exponentially as  $\langle \theta^2 \rangle \propto \langle (\nabla \theta)^2 \rangle \propto \exp(-\beta_0 t)$ , with  $\beta_0 = 2DK^2$ .

The presence of polymers causes a strong enhancement of the mixing, which is illustrated by the vertical sections of  $\theta$  shown in Fig. 9. In particular, we observe the formation of thin scalar filaments, which rapidly transfer the scalar fluctuations to small dissipative scales. This process strongly enhances the mixing efficiency with respect to the molecular diffusion. A quantitative measure

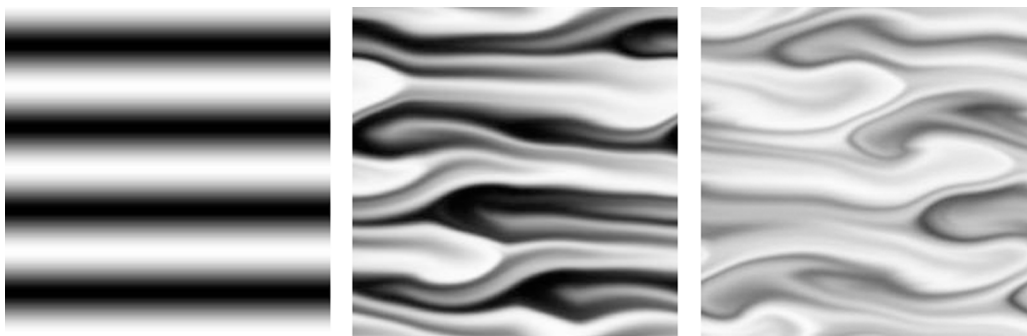


FIG. 9. Vertical section in the  $x$ - $z$  plane at fixed  $y = 0$  of the scalar field  $\theta$  for the 3D simulation with  $\eta = 8$  at different times. From left to right:  $t = 0$ ,  $t = 32T_0$ ,  $t = 64T_0$ .

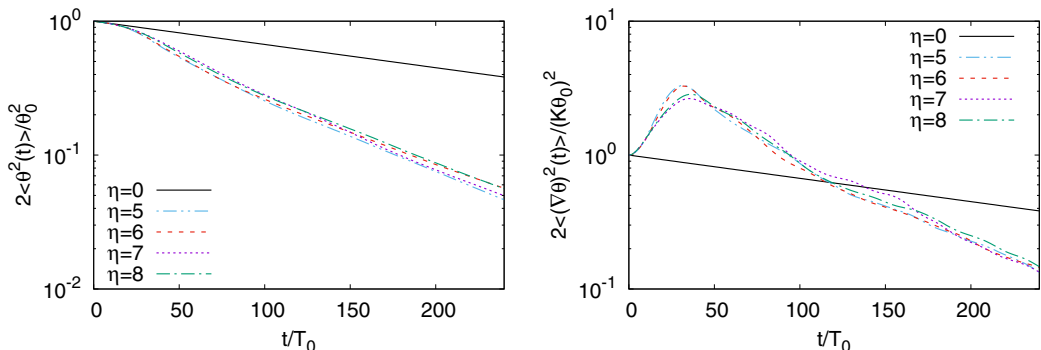


FIG. 10. Decay of the variance of the scalar field  $\langle \theta^2 \rangle$  (left panel) and of the scalar gradients  $\langle (\nabla\theta)^2 \rangle$  (right panel) for the different values of  $\eta$  in 3D simulations. Solid black line represents the diffusive exponential decay in absence of polymers.

of the mixing is provided by the temporal evolution of the variance of  $\theta$  and  $\nabla\theta$  shown in Fig. 10. Here and in the following, the results presented are averaged over 13 independent simulations of Eq. (8), starting from the same initial condition  $\theta(\mathbf{x}, 0)$  with different velocity fields. The decay of  $\langle \theta^2 \rangle$  in the chaotic flow induced by the polymers is much faster with respect to the case  $\eta = 0$ . The same result is observed for the long-time decay of the variance of scalar gradients  $\langle (\nabla\theta)^2 \rangle$ , even though the chaotic advection of the scalar field causes an initial increase of its gradients (this effect is clearly seen in Fig 9). For the concentration values considered in our study, we do not observe a strong dependence of the mixing efficiency on  $\eta$ .

The instantaneous exponential decay rate of the scalar variance  $\beta_p = -\frac{d}{dt} \log\langle \theta^2 \rangle$  can be written, using Eq. (8), as

$$\beta_p(t) = -\frac{d}{dt} \log\langle \theta^2 \rangle = 2D \frac{\langle (\nabla\theta)^2 \rangle}{\langle \theta^2 \rangle}, \quad (9)$$

which can be directly compared with the decay rate due to molecular diffusion  $\beta_0 = 2DK^2$ .

The decay rate  $\beta_p$  reaches a maximum value after a very short time, corresponding to the maximum development of thin filaments of the scalar field. At longer time, since both  $\langle \theta^2 \rangle$  and  $\langle (\nabla\theta)^2 \rangle$  decay exponentially,  $\beta_p$  approaches an almost constant value, about three times larger than  $\beta_0$  (see Fig. 11) which quantifies the increased mixing efficiency. We note that the ratio  $\beta_p/\beta_0$  is

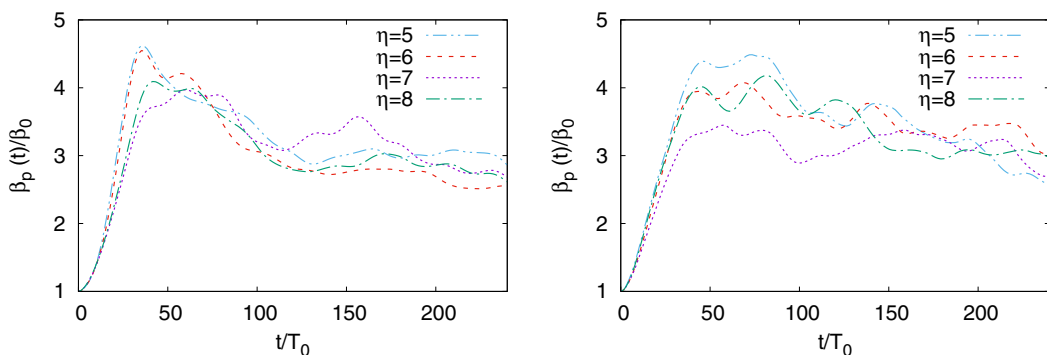


FIG. 11. Instantaneous exponential decay rate  $\beta_p(t)$  for different values of  $\eta$  in 3D simulations (left panel) and 2D simulations (right panel).

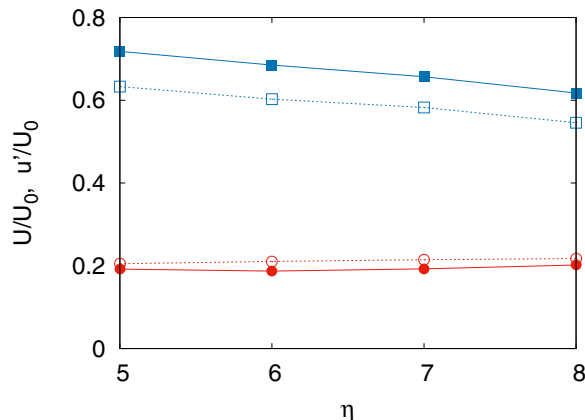


FIG. 12. Amplitudes of mean velocity profiles  $U$  (blue squares) and rms velocity fluctuations  $u'_{\text{rms}}$  (red circles) as a function of  $\eta$  in 3D (filled symbol) and 2D (empty symbols) simulations.

proportional to the square of the ratio between the large scale of the scalar field  $1/K$  and the typical scale of its gradients  $(\langle \theta^2 \rangle / \langle (\nabla \theta)^2 \rangle)^{1/2}$ .

### E. Comparison between 2D and 3D

The results presented so far show that the properties of the chaotic flow, which is obtained from 3D numerical simulations of the model (1) for a dilute solution of rigid rods, are qualitatively similar to those reported in previous numerical studies in 2D [15,16]. In particular, we found that the fluctuations of the  $y$  component of the velocity  $u_y$ , which is transverse both to the streamwise direction of the mean flow  $x$  and to the direction of its gradient  $z$ , are considerably smaller than those of  $u_x$  and  $u_z$  (see Fig. 4). This confirms that the dynamics of the three-dimensional system is substantially two-dimensional, and that the properties of the chaotic flow are qualitatively independent on its dimensionality.

To make a quantitative comparison, we performed an additional set of 2D simulations of Eq. (1) in the  $(x, z)$  plane with the same parameters of the 3D simulations. The comparison of the mean flow and velocity fluctuations, reported in Fig. 12, shows that the effects of polymers are more pronounced in 2D than in 3D. At fixed value of the polymer concentration  $\eta$ , we find that the velocity fluctuations are more intense in 2D than in 3D. Similarly, the reduction of the amplitude  $U$  of the mean flow with respect to the laminar solution  $U_0$  is stronger in 2D than in 3D. It is worth to notice that 2D and 3D curves of  $U$  and  $u'$  as a function of  $\eta$  are almost parallel, which indicates that the effect of dimensionality is systematic and it is independent on  $\eta$ .

The comparison of the momentum balance is reported in Fig. 5. Also in this case we observe that the values of the friction factor in 2D are systematically higher than in 3D at fixed  $\eta$ . We find that the drag enhancement is mostly due to the increase of the polymer stress, with a subdominant contribution due to the increase of the viscous stress. The combined effect of increased friction factor and reduced Reynolds number is clearly visible in Fig. 6, in which the deviation from the Newtonian point  $f = 1$  is stronger for the 2D simulations. In the energy balance, the reduction of the amplitude of the mean flow causes a reduction of the energy injection rate  $\varepsilon_I$  in 2D simulations with respect to the 3D ones at fixed  $\eta$  (see Fig. 7). This phenomenon is balanced by a reduction of the viscous dissipation rate  $\varepsilon_v$ , while the energy dissipation due to polymers remains almost unchanged.

In summary, we can conclude that the effects of rodlike polymers in viscous flows in three-dimensions is weaker than in two dimensions. The origin of this difference is probably due to the different rotational degrees of freedom of the rods. In 2D, the rotation of the polymers can occur

only in the  $x$ - $z$  plane. This implies that, during the rotation, polymers are oriented in the direction of the gradient of the mean flow (the  $z$  direction). Conversely, in 3D they can rotate also in the  $x$ - $y$  plane. Indeed we observed that in the stationary regime the average values of  $R_{22}$  and  $R_{33}$  are very similar. Nonetheless, the consequences of polymer rotations in the  $x$ - $z$  and  $x$ - $y$  planes on the polymer stress tensor  $\sigma_{ij}$  are very different. We remind that  $\sigma_{ij}$  is proportional to the product of the configuration tensor  $R_{ij}$  and the velocity gradient tensor  $\partial_i u_j$ . In the case of the laminar Kolmogorov flow  $\mathbf{u}(\mathbf{x}) = [U_0 \cos(Kz), 0, 0]$ , the only component of the velocity gradient which is nonzero is  $\partial_3 u_1$ . As a consequence, there is no stress induced by rotations in the  $x$ - $y$  plane (allowed only in 3D). In the case of the chaotic flow, the gradients of velocity in the  $y$  direction originates only from the fluctuating part of the velocity field, therefore they are significantly smaller than those in the  $z$  direction. As a result, the polymer stress in 3D is on average weaker than in 2D flow with the same  $\eta$ .

An heuristic estimate of the dimensional dependence of the average polymer stress can be obtained from the formal expression of the stress tensor in  $d$  dimensions [21]  $\sigma_{ij} = 2d\nu\eta R_{ij}(\partial_i u_k)R_{kl}$ , which is derived under the assumption of isotropy of the conformation tensor  $R_{ij} = \delta_{ij}/d$  in the limit of zero shear. Even though this hypothesis is not fulfilled in the case of the Kolmogorov flow, since the nonvanishing mean shear induces a preferential alignment of the rods in the direction of the mean flow, one can argue that simulations in 2D and 3D can be simply mapped by rescaling the polymer concentration as  $\eta^{2D} = (2/3)\eta^{3D}$ . We tested this prediction by comparing two simulations in 2D, with reduced parameters  $\eta^{2D} = 4$  and  $\eta^{2D} = 5.33$ , with the corresponding simulations in 3D with  $\eta^{3D} = 6$  and  $\eta^{3D} = 8$ . In both cases, we found that the rescaling of the concentration reduces the difference between the amplitude of the mean flow in 2D and 3D below 3%. Therefore, although the rescaling is not exact, it provides a simple and useful empirical rule to translate 2D results for 3D applications, at least for this flow. This mapping supports the interpretation of the dimensional effects reported in our study in terms of the different rotational degrees of freedom of the rods.

Finally, we compare the mixing properties of 2D and 3D flows by integrating the transport Eq. (8) for a two-dimensional scalar field  $\theta$  transported by the 2D flow. Initial conditions and diffusion coefficient are identical to those of 3D simulations. The values of the instantaneous exponential decay rate  $\beta_p(t)$  obtained in the 2D simulations are shown in Fig. 11. They are very similar to those obtained in 3D simulations. This is in agreement with the observation that the intensity of velocity fluctuations, which causes the mixing, is very similar as well (see Fig. 12).

## V. CONCLUSIONS

We studied the dynamics of rigid rodlike polymer solutions at low Reynolds numbers by means of direct numerical simulations of a rheological model both in 2D and in 3D. We found that the presence of polymers induces a chaotic, turbulent-like flow with increased flow resistance and enhanced mixing efficiency at Reynolds numbers at which the laminar solution for the Newtonian fluid without polymers is linearly stable. The phenomenology observed is qualitatively independent on the dimensionality, but we found that, for the same values of the parameters, the effects are stronger in the 2D case. This difference is explained in terms of the different rotational degrees of freedom of the rods.

Future numerical works in more complex and realistic geometries would open the possibility to a direct comparison with the results of laboratory experiments. A viable experimental realization could be performed with a dilute solution of polymers of length  $\ell \approx 2\text{--}5 \mu\text{m}$  (e.g., xanthan gum) at concentrations of about 100 wppm, in a microchannel of width  $L \approx 2 \text{ mm}$  with velocity of the order of  $U \approx 6 \text{ mm/s}$ . The scales and the setup are similar to the ones considered in elastic turbulence experiments [5,34,35]. For the comparison between models and experiments it would be useful to investigate also the role of rotational diffusion, which is expected to influence the dynamics at moderate rotational Péclet numbers.

## ACKNOWLEDGMENTS

We acknowledge HPC CINECA for computing resources (INFN-CINECA Grant No. INFN21-FieldTurb). We acknowledge support from the Departments of Excellence grant (MIUR).

---

- [1] B. A. Toms, Some observations on the flow of linear polymer solutions through straight tubes at large Reynolds numbers, in *Proceedings of the International Congress on Rheology* (1949), Vol. 135, pp. 135–141.
- [2] A. Gyr and H. W. Bewersdorff, *Drag Reduction of Turbulent Flows by Additives* (Springer Science & Business Media, Cham, 2013), Vol. 32.
- [3] K. R. Sreenivasan and C. M. White, The onset of drag reduction by dilute polymer additives, and the maximum drag reduction asymptote, *J. Fluid Mech.* **409**, 149 (2000).
- [4] C. M. White and M. G. Mungal, Mechanics and prediction of turbulent drag reduction with polymer additives, *Annu. Rev. Fluid Mech.* **40**, 235 (2008).
- [5] A. Groisman and V. Steinberg, Elastic turbulence in a polymer solution flow, *Nature (London)* **405**, 53 (2000).
- [6] A. Groisman and V. Steinberg, Efficient mixing at low Reynolds numbers using polymer additives, *Nature (London)* **410**, 905 (2001).
- [7] S. Berti, A. Bistagnino, G. Boffetta, A. Celani, and S. Musacchio, Two-dimensional elastic turbulence, *Phys. Rev. E* **77**, 055306 (2008).
- [8] B. Qin and P. E. Arratia, Characterizing elastic turbulence in channel flows at low Reynolds number, *Phys. Rev. Fluids* **2**, 083302 (2017).
- [9] A. S. Pereira, R. M. Andrade, and E. J. Soares, Drag reduction induced by flexible and rigid molecules in a turbulent flow into a rotating cylindrical double gap device: Comparison between Poly (ethylene oxide), Polyacrylamide, and Xanthan Gum, *J. Non-Newtonian Fluid Mech.* **202**, 72 (2013).
- [10] P. S. Virk, D. C. Sherman, and D. L. Waggener, Additive equivalence during turbulent drag reduction, *AIChE J.* **43**, 3257 (1997).
- [11] J. S. Paschkewitz, Y. Dubief, C. D. Dimitropoulos, E. S. G. Shaqfeh, and P. Moin, Numerical simulation of turbulent drag reduction using rigid fibres, *J. Fluid Mech.* **518**, 281 (2004).
- [12] R. Benzi, E. S. C. Ching, T. S. Lo, V. S. L'vov, and I. Procaccia, Additive equivalence in turbulent drag reduction by flexible and rodlike polymers, *Phys. Rev. E* **72**, 016305 (2005).
- [13] J. J. J. Gillissen, Polymer flexibility and turbulent drag reduction, *Phys. Rev. E* **78**, 046311 (2008).
- [14] L. Warwaruk and S. Ghaemi, Near-wall lubricating layer in drag-reduced flows of rigid polymers, *Phys. Rev. Fluids* **7**, 064605 (2022).
- [15] E. L. C. VIM. Plan, S. Musacchio, and D. Vincenzi, Emergence of chaos in a viscous solution of rods, *Phys. Rev. E* **96**, 053108 (2017).
- [16] S. Musacchio, M. Cencini, E. L. C. VIM. Plan, and D Vincenzi, Enhancement of mixing by rodlike polymers, *Eur. Phys. J. E* **41**, 84 (2018).
- [17] R. H. Kraichnan, Inertial ranges in two-dimensional turbulence, *Phys. Fluids* **10**, 1417 (1967).
- [18] G. Boffetta and R. E. Ecke, Two-dimensional turbulence, *Annu. Rev. Fluid Mech.* **44**, 427 (2012).
- [19] G. Boffetta, M. Borgnino, and S. Musacchio, Scaling of rayleigh-taylor mixing in porous media, *Phys. Rev. Fluids* **5**, 062501(R) (2020).
- [20] M. Borgnino, G. Boffetta, and S. Musacchio, Dimensional transition in Darcy-Rayleigh-Taylor mixing, *Phys. Rev. Fluids* **6**, 074501 (2021).
- [21] M. Doi and S. F. Edwards, *The Theory of Polymer Dynamics* (Oxford University Press, Oxford, UK, 1988), Vol. 73.
- [22] J. J. J. Gillissen, B. J. Boersma, P. H. Mortensen, and H. I. Andersson, The stress generated by non-Brownian fibers in turbulent channel flow simulations, *Phys. Fluids* **19**, 115107 (2007).
- [23] A. H. Kumar, S. J. Thomson, T. R. Powers, and D. M. Harris, Taylor dispersion of elongated rods, *Phys. Rev. Fluids* **6**, 094501 (2021).

- [24] R. Benzi, E. S. C. Ching, E. De Angelis, and I. Procaccia, Comparison of theory and direct numerical simulations of drag reduction by rodlike polymers in turbulent channel flows, [Phys. Rev. E \*\*77\*\*, 046309 \(2008\)](#).
- [25] Y. Amarouchene, D. Bonn, H. Kellay, T. S. Lo, V. S. L'vov, and I. Procaccia, Reynolds number dependence of drag reduction by rodlike polymers, [Phys. Fluids \*\*20\*\*, 065108 \(2008\)](#).
- [26] L. D. Meshalkin and I. G. Sinai, Investigation of the stability of a stationary solution of a system of equations for the plane movement of an incompressible viscous liquid, [J. Appl. Math. Mech. \*\*25\*\*, 1700 \(1961\)](#).
- [27] S. Musacchio and G. Boffetta, Turbulent channel without boundaries: The periodic Kolmogorov flow, [Phys. Rev. E \*\*89\*\*, 023004 \(2014\)](#).
- [28] G. Boffetta, A. Celani, and A. Mazzino, Drag reduction in the turbulent Kolmogorov flow, [Phys. Rev. E \*\*71\*\*, 036307 \(2005\)](#).
- [29] A. Sozza, M. Cencini, S. Musacchio, and G. Boffetta, Drag enhancement in a dusty Kolmogorov flow, [Phys. Rev. Fluids \*\*5\*\*, 094302 \(2020\)](#).
- [30] J. P. Boyd, *Chebyshev and Fourier Spectral Methods* (Dover Publication, Mineola, NY, 2001).
- [31] R. Sureshkumar and A. N. Beris, Effect of artificial stress diffusivity on the stability of numerical calculations and the flow dynamics of time-dependent viscoelastic flows, [J. Non-Newtonian Fluid Mech. \*\*60\*\*, 53 \(1995\)](#).
- [32] S. Berti and G. Boffetta, Elastic waves and transition to elastic turbulence in a two-dimensional viscoelastic Kolmogorov flow, [Phys. Rev. E \*\*82\*\*, 036314 \(2010\)](#).
- [33] A. Varshney and V. Steinberg, Elastic Alfvén waves in elastic turbulence, [Nat. Commun. \*\*10\*\*, 652 \(2019\)](#).
- [34] A. Groisman and V. Steinberg, Elastic turbulence in curvilinear flows of polymer solutions, [New J. Phys. \*\*6\*\*, 29 \(2004\)](#).
- [35] V. Steinberg, Elastic turbulence: An experimental view on inertialess random flow, [Annu. Rev. Fluid Mech. \*\*53\*\*, 27 \(2021\)](#).